The Distribution of Middle Tropospheric Carbon Monoxide During Early October 1984

Henry G. Reichle, Jr., Vickie S. Connors, and H. Andrew Wallio

Atmospheric Sciences Division
NASA Langley Research Center

J. Alvin Holland

Flight Electronics Division
NASA Langley Research Center

Robert T. Sherrill

Systems Engineering Division
NASA Langley Research Center

Joseph C. Casas

SpaceTec Ventures, Incorporated

Barbara B. Gormsen

ST Systems Corporation

Abstract

The distribution of middle tropospheric carbon monoxide measured by the Measurement of Air Pollution from Satellites (MAPS) instrument carried aboard the space shuttle during October 1984 is reported. The data represent average mixing ratios in the middle troposphere between 57°N and 57°S. Approximately 75,000 individual carbon monoxide measurements were obtained during the 9 day mission. The data are presented in the form of maps that show the carbon monoxide mixing ratios averaged over 5° latitude by 5° longitude areas for 6 days of the mission. Comparisons with concurrent, direct measurements taken aboard aircraft show that the inferred concentrations are systematically low by from 20 to 40 percent depending upon which direct measurement calibration standard is used. The data show that there are very large CO sources resulting from biomass burning over South America and southern Africa. Measured mixing ratios were high over northeast Asia and were highly variable over Europe.

Introduction

Carbon monoxide (CO) is produced as a result of both natural and anthropogenic activities. The primary natural source is thought to result from the oxidation of methane and other hydrocarbons, while the primary anthropogenic sources are technological activities which are concentrated in the Northern Hemisphere and biomass burning which is concentrated in the tropical regions. It now appears that the natural and anthropogenic sources are of nearly equal magnitude (Logan et al., 1981). Because CO is by far the largest sink for the hydroxyl radical in the troposphere (Logan et al., 1981) and because the hydroxyl radical is the principal oxidizer for reduced species in the troposphere, these large anthropogenic emissions could modify the chemical balance of the troposphere and cause the mixing ratios of the reduced species to increase. For example, one of these species, methane, is both a greenhouse gas and a major source of water vapor in the stratosphere. As a result, the large anthropogenic emissions of CO could influence both the climate and the chemistry of stratospheric ozone.

This paper presents the CO data obtained by the Measurement of Air Pollution from Satellites (MAPS) experiment during its second flight aboard the space shuttle. The CO mixing ratio data were obtained during the period from October 5 to October 13, 1984, over all longitudes between 57°N latitude and 57°S latitude. The data represent the average mixing ratio of CO between the top of the mixing layer and the tropopause. A detailed description of the instrument technique and calibration, the data reduction procedures, and the measurement results for the first space shuttle flight of the MAPS experiment, which occurred during November 1981, has been reported (Reichle et al., 1986). This paper briefly discusses the earlier methods, presents information on changes to the instrument and data reduction technique, and reports the

results of 85 hours of CO mixing ratio measurements obtained during this flight.

The global distribution of CO has been the subject of study for about twenty years. Seiler [1974] summarized the state of knowledge at that time. Basically, it appeared that the CO mixing ratio was higher in the Northern Hemisphere than in the Southern Hemisphere with maximum values being found near the surface at northern mid-latitudes. In general this still appears to be the case. The seasonally averaged mixing ratio is about 120 ppbv at 45°N and 60 ppbv near 45°S (Logan et al., 1981). Since 1974 it has become clear that there is a seasonal variation in the CO mixing ratio with maximum values occurring in local spring and minimum values occurring in local fall (Khalil and Rasmussen, 1984; Seiler et al., 1984; Fraser et al., 1986). Both flights of the MAPS experiment occurred during Northern Hemisphere fall when the north-south gradient should be near its minimum value. In addition to the seasonal variation, it has been recently estimated that the CO mixing ratio has been increasing at a rate of about one to two percent per year (Rinsland and Levine, 1985; Khalil and Rasmussen, 1988). Because the lifetime of CO is on the order of 30 to 90 days, depending upon the altitude and season, it seemed that the gas would be more or less uniformly distributed with longitude. However, the data reported by Reichle et al. [1986] have clearly demonstrated that strong gradients with longitude are present.

The MAPS Instrument

The MAPS experiment is comprised of a nadir-viewing instrument designed to measure the global distribution of middle tropospheric CO. The instrument uses the gas filter correlation technique to maintain high radiation throughput and high effective spectral resolution in the 4.67 μm fundamental band of CO. The MAPS instrument is similar in principle to the selective

chopper radiometer (Able et al., 1970); however, the MAPS instrument uses the automatic gain control technique described by Ward and Zwick [1975].
As shown schematically in Figure 1, the upwelling radiation is gathered by the optical system and is simultaneously directed by a system of beam splitters through three gas-filled cells to the detectors for each of the three signal channels. One channel, called the V channel, has a gas cell which contains only helium which does not interact with the collected radiation, and thus the output signal from this detector provides a measure of the brightness temperature of the target surface. During the first flight, the second and the third gas cells were both filled with CO; however, for reasons which will be discussed later, for the 1984 flight, the second gas cell was filled with CO and the third gas cell was filled with nitrous oxide (N_2O). The output signals of the detectors behind the second and third gas cells are each electronically subtracted from the output signal of the V Channel detector to form signals for the ΔV and $\Delta V'$ channels, respectively. These difference signals are strongly related to the degree of correlation between the spectrum of the gas contained in the gas-filled cells and the spectrum of the collected radiation and, therefore, provide the basis for determining the amount of CO and N_2O in the atmosphere (Reichle et al., 1986). The primary characteristics of the instrument and details of the composition of the gas in the cells are contained in Table 1.

The configuration of the MAPS instrument package, shown in Figure 2, includes the following: the optical subassembly, which contains all of the optical elements, blackbodies, gas cells, detectors, preamplifiers, and a balance/calibrate unit; the electronics subassembly, which houses the signal processing and control circuits, data-handling circuits, balance/calibrate circuits, mode-sequencing and control circuits, and power-conditioning

circuits; the flight magnetic tape recorder subassembly, which records the scientific data for all three channels and the housekeeping data during the mission; and the aerial camera subassembly, which provides correlative cloud cover photographs of the subsatellite ground track during daylight portions of flight.

Signal Function

In the 4.67 μm region of the spectrum the primary upwelling radiation is the thermal radiation emitted by the earth-atmosphere system. As a result, the signal depends not only on the amount of CO in the atmosphere but also on the altitude at which it is located. If we define the radiometric signal received at the detectors as ΔL, then ΔL can be expressed as

$$\Delta L = \int_{p_s}^{0} SF \, d(\ln p) \tag{1}$$

where P_s is the surface pressure and SF is the signal function. For an atmosphere in local thermodynamic equilibrium

$$SF = \int_{\Delta\nu} a(p)\tau^{p,0}[G - L_a[T(p)]][\tau_{vac} - \tau_{gas}]\frac{RT(p)}{mg}F d\nu$$

where

$a(p)$ = the absorption per unit pressure

$\tau^{p,0}$ = the transmittance from the pressure p to the top of the atmosphere

G = the emissivity of the surface times the Planck Function at the surface temperature

$L_a[T(p)]$ = the blackbody radiance for the temperature T(p)

τ_{vac} = the effective transmission of the vacuum leg (the helium filled cell of the instrument)

τ_{gas} = monochromatic transmission of the gas cell

R = the universal gas constant

m = molecular weight

g = acceleration of gravity

F = instrument response function.

The instrument spectral characteristics are determined by the product $[\tau_{vac} - \tau_{gas}]F$. In this instrument, τ_{vac} is set during the balancing process and is maintained by an electronic servo system; τ_{gas} is determined by the gas cell pressure and temperature, the concentration of the gas in the cell and the cell length; and F is primarily controlled by the broadband filter. The passband of this filter was chosen to block out most of the lines of the overlapping carbon dioxide and N_2O bands.

For the second flight, as noted earlier, one of the gas cells in the instrument contained N_2O. The cell conditions were chosen so that the signal function for the N_2O channel would closely match the signal function of the CO channel. The cell conditions for the CO channel were the same as those flown in the high pressure channel (ΔV) of the first flight. The signal functions for the two channels are shown in Figure 3, where it can be seen that the signal functions are quite closely matched.

Instrument Calibration

The instrument was calibrated in a vacuum chamber at a variety of instrument temperatures before and after the flight. The calibration method was the same as that used during the calibration that followed the 1981 flight. The pre and post flight calibration data agree to about 1 percent for the ΔV and $\Delta V'$ channels and 3 percent for the V channel, and they show that no significant changes in the calibration occurred between the flights. During

the calibration, mixtures of either mixtures of either CO or N_2O in nitrogen were placed in a cell in front of the instrument. The temperature of a blackbody target beyond the cell was then stepped through a series of temperatures, and the output voltages were recorded for the various gas mixtures, target temperatures, and instrument temperature combinations.

The same line-by-line radiative transfer program that was used in the atmospheric radiative transfer calculations was used to calculate theoretical radiometric signals that corresponded to the test conditions. Plots of the observed voltage signals, as a function of the theoretically derived radiometric signals, allowed the instrument calibration constants to be determined as a function of instrument temperature. The test conditions for the instrumentcalibration are outlined in Table 2.

Carefully planned calibrations and space-viewing data collection periods were obtained frequently during this flight. The temperature of the shuttle coolant loop (which controls the instrument temperature) was much more stable during this flight than it was on the 1981 flight, and as a result it was not necessary to correct the data reported here for the effects of temperature changes between inflight calibrations. This was verified through the use of the data obtained while the instrument was viewing deep space.

Data Reduction

The data reduction process proceeds along three parallel paths. In the first path, the recorded digital signals from the data channels and from the housekeeping channels are combined with the ground calibration data to yield radiometric signals as a function of time. In the second path, line-by-line radiance calculations are performed to generate regression coefficients based on a set of atmospheric models that describe the variation of temperature and

humidity with height. This technique is described by Wallio et al. [1983] and is discussed in this application by Reichle et al. [1986]. Because this flight spanned a greater range of latitude, a new set of atmospheric models was required. These models will be discussed in a later section of this paper. In the third path of the data reduction, meteorological analyses for the flight period are combined with the signal function to form a set of gridded, vertically weighted atmospheric temperatures. This is then combined with both the spacecraft ephemeris data and a terrain analysis to yield a file of weighted atmospheric temperature and underlying surface type for each geographical location at which CO data were acquired.

At this point the three paths converge. First the regression coefficient sets and the temperature/terrain files are combined to produce a set of interpolated regression coefficients for each data point. These regression coefficients are then used in combination with the radiometric data produced in path one to produce inferred CO mixing ratios. Finally, the data are filtered to remove data points that are strongly influenced by the presence of clouds in the field of view.

With two exceptions, the process outlined above is essentially the same as that used for the 1981 flight. First, new atmospheric models were used, and second, a new method for filtering out the effects of clouds was developed.

The Atmospheric Models

A set of 11 atmospheric models that were representative of the meteorological conditions that existed from October 5 through October 13, 1984, was developed. Each model consists of a vertical profile of temperature, geopotential height, and mixing ratios for CO, carbon dioxide,

N_2O, water vapor, and ozone. Carbon dioxide and N_2O are assumed to be uniformly mixed at 330 ppmv and 301 ppbv respectively. Because ozone variations cause only very small errors in the inferred CO mixing ratio, a single ozone profile was used in all of the models. Of the five gases, water vapor is the most variable in space and time. Each of the 11 models has a distinct water vapor mixing ratio profile representing climatological conditions for that model. The vertical profiles of temperature and water vapor for several of the models are shown in Figure 4a and 4b. Some intermediate models have been omitted for clarity. Table 3 shows the surface and tropopause characteristics for all of the models.

Cloud Filtering

The inferred CO data are valid only if the field of view is cloud free or if any clouds present are located in the mixing layer. Following the inference of the CO mixing ratios, it is necessary to reject those points that are cloud contaminated. In the previously reported data this was done by a subjective method that involved examining each frame of the camera film that was acquired along the track. This method was highly labor intensive and not at all suitable for processing large amounts of data. Consequently, a new method was developed, tested, and applied to the data reported here.

The inclusion of a N_2O channel was originally suggested by Dr. John Houghton of Oxford University (personal communication, 1978), who suggested that this channel could be used to determine the effective temperature of the infrared active CO. Although the data from this channel have not been used for this purpose the signals from the N_2O channel now form the basis of an objective, automated method of filtering cloud contaminated data. In addition, current studies indicate that further analysis of the N_2O data will allow the development of

a technique that will both correct many systematic and random errors and recover some cloud contaminated data.

The inversion algorithms used to infer the CO and N_2O atmospheric mixing ratios from the radiometric measurements of the three channels assume that the instrument is sensing signals from the ground-atmosphere system in a cloud free column. If clouds are present, the instrument senses radiation from both the surface and from the cloud tops; and as a result, the inferred CO and N_2O mixing ratios are too large. N_2O is assumed to be vertically, horizontally, and temporally uniformly mixed in the troposphere. Thus, any inferred N_2O mixing ratio sufficiently greater than the average inferred for the uniform atmospheric value can be considered to be inferred from cloud contaminated data, and the corresponding CO mixing ratio is also assumed to be erroneous because of cloud contamination. In Figure 5 the dotted curve is the cumulative frequency distribution of the inferred N_2O mixing ratio where the vertical axis represents the number of N_2O data points inferred at a particular concentration. The distribution curve has a peak at about 210 ppbv and a large tail at higher values of the N_2O mixing ratio. The measured N_2O mixing ratio was expected to peak at 301 ppbv (Weiss, 1981), not 210 ppbv, and we attribute this inconsistency to a systematic error in calculating the spectral response of the N_2O gas channel. For our purposes of cloud filtering this offset is not crucial since we are only trying to isolate those data points that are significantly above the mean retrieval value. The solid curve in Figure 5 is a Gaussian fit to the left hand side of the measured cumulative distribution function. The fit is a weighted least squares, with more weight applied toward the middle and peak of the function. The mean of the Gaussian fit is 210.2 ppbv and the standard deviation is 20.3 ppbv. If N_2O is uniformally distributed as assumed, this standard deviation gives an initial

estimate of the random error of the measurement system, regardless of the error in the measured mean mixing ratio that might be caused by a bias or a linear shift. This random error is on the order of ±10 percent. Mixing ratio values of the N_2O distributed to the left of the mean and above the plotted Gaussian are assumed to be random errors from the mean. These values are larger than the fitted Gaussian because there is more than one Gaussian distribution describing the measurement errors and these error distributions will vary with time during the experiment. Mixing ratio values of the N_2O distributed to the right and above the plotted Gaussian are assumed to be cloud contaminated measurements.

The CO mixing ratio data presented in this paper are filtered using a N_2O value of 231 ppbv, i.e., 10 percent greater than the mean retrieval value of 210 ppbv. If the inferred N_2O mixing ratio is greater than 231 ppbv, then the CO data are assumed to be cloud contaminated and are dropped. The data from a single orbit and the results of the application of the N_2O filter technique are illustrated in Figure 6. Figure 6a is a plot of the inferred CO mixing ratio before any filtering is applied. Figure 6b shows the same data after applying the N_2O filter to remove the cloud contaminated data. Figure 6c shows the suborbital ground track for this orbit of data. As can be seen by comparing Figure 6a with Figure 6b, the cloud filter not only removes all the spuriously high values of the CO mixing ratios but also removes the very sharp spikes associated with large clouds passing through the field of view of the instrument. The operation of the filtering technique was checked through a careful review of the cloud cover as shown by the sub-satellite photography taken by the MAPS camera. The photographs were checked for situations in which the filter indicated either the presence of clouds or the absence of clouds. The filter was found to be operating correctly in both cases. On the

basis of the photography, it appears that the cutoff limit might have been set somewhat higher than 231 ppbv, and thereby increasing the number of CO data points retained, however it was decided that a conservative approach would be taken.

Error Estimates

Both theoretical and experimental methods were used to define the errors contained in the data reported here. In the first method, numerical simulations using the line-by-line radiative transfer model were carried out to estimate the errors resulting from either uncertainties or errors in various input data or from instrument errors. A detailed discussion of these analyses is given by Reichle et al. [1986], and the results of the analyses as they apply to these data will be given in the next section. In the second method, aircraft were flown under the spacecraft. These aircraft carried either air sampling systems for the direct measurement of CO or a gas filter radiometer similar to the one carried aboard the space shuttle. The results of the aircraft measurements and the spacecraft measurements are then compared.

Theoretical Error Estimates

The most significant difference between the first and second MAPS flights was that for the second flight the $\Delta V'$ channel was filled with N_2O rather than CO. A summary of the theoretical error estimates for the experiment is given in Table 4. The changes in the error estimates for the second flight are first that the atmospheric N_2O mixing ratio used in the derivation of the CO inversion coefficients has been taken to be 301 ppbv and second that no instrument bias shift was observed during this flight. The total random error as calculated for Table 4 should represent a near upper limit. An experimental estimate of the random error for the N_2O channel is discussed in the section on cloud filtering and was found to be about 10 percent. Since

the instrumentation and total data reduction process is the same for both channels, it is expected that the random error for the CO channel will also be about 10 percent. As mentioned earlier, the bias or variable linear shifts observed in the inferred N_2O mixing ratio will, with further analysis, provide a means of removing systematic errors in the measurements of the CO mixing ratio.

Experimental Assessment of Error

Three aircraft flew correlative measurement missions in conjunction with this flight of the MAPS experiment. The NASA Convair 990 flew two missions during the early part of the 9 day flight period. It carried air sampling equipment and measured radiometric surface temperature, air temperature, and dew point near Albuquerque, New Mexico and over the ocean west of Baja California. A NASA Learjet flew seven flights near the western and southern coasts of Florida. It was equipped with a gas filter radiometer similar to the shuttle instrument, air sampling equipment, a surface temperature radiometer, a total air temperature probe and a dewpoint/frostpoint hygrometer. Because of sample line leakage problems, the CO data derived from the sample bottles aboard this aircraft were not usable as correlative measurements. The third aircraft was a Lufthansa air freighter that flew from Frankfurt, West Germany to Sao Paulo, Brazil and return with an intermediate stop at Dakar, Senegal. The measurement system on the Lufthansa air freighter was operated by personnel of the Fraunhoffer Institute for Atmospheric Environmental Research under the direction of Dr. Wolfgang Seiler. This group conducted a comprehensive set of gas analyses, including the measurement of CO at 1 minute intervals.

The data from the Convair 990 and the Learjet, along with the corresponding spacecraft measurements, are shown in Table 5. Table 5 shows

that the gas filter radiometer aboard the Learjet generally yielded CO values that are about 15 percent lower than the values measured by the spacecraft instrument. Since the same data reduction method was used for both instruments, it is not likely that the discrepancy was introduced there, but rather it is an effect introduced by a difference in the calibration method. The major difference was that two different cell lengths (about two cm for the spacecraft instrument and one-half meter for the aircraft instrument) were used in the calibrations. This results in the use of different mixing ratios for the calibration gases with possibly different errors in the gas composition. This situation has been changed, and in the future both instruments will be calibrated using the same 1 meter calibration cell and the same gas mixtures.

The data acquired by the Convair 990 aircraft, shown in Table 5, are the mean and standard deviation of the 10 measurements taken on each flight between the altitudes of 4.5 km and 9.5 km in a nearly vertical profile at the indicated locations. It can be seen that the spacecraft measurements are about 20 (28°N, 125°W) to 40 (35°N, 105°W) percent lower than the values derived by the direct aircraft measurements.

The third set of aircraft measurements were obtained by the Lufthansa air freighter. The aircraft flew at an altitude between 8.2 and 9.5 km for essentially the entire mission. This placed it in the free troposphere near the altitude of the peak of the MAPS signal function. It very nearly followed a great circle route on the outbound leg from Frankfurt to Sao Paulo and on the return leg from Sao Paulo to Dakar. On the leg from Dakar to Frankfurt, its route was to the west of a great circle because of wind conditions along the route. The aircraft left Frankfurt at 17:00 on October 6 and arrived at

Sao Paulo at 08:00 on October 7 (all times are Universal Times). It then left Sao Paulo at 00:00 on October 8 and arrived at Frankfurt at 13:30 on October 8.

The times of the Lufthansa aircraft and corresponding spacecraft data acquisition are shown in Table 6. The aircraft measurement campaign was divided into four segments, each of which was compared in space and time with the location of the space shuttle. The spacecraft data, associated with the Frankfurt-Dakar aircraft data, were acquired during several orbits over a period of 5 hours. The aircraft measurements lagged those from space by only 8 hours. On the Dakar-Sao Paulo segment, the northbound spacecraft and southbound aircraft flew nearly coincident flight tracks. At 5:30 on October 7, the spacecraft passed 300 km to the west of the aircraft over the Atlantic Ocean east of Recife, Brazil. During the Sao Pualo-Dakar aircraft leg on October 8, the ground track of the spacecraft was even closer to that of the aircraft. At about 11°N off the Senegal coast, the northbound spacecraft passed 100 km west of the northbound aircraft.

The comparison of these two data sets has posed a considerable challenge. Clearly, the best data from the point of view of space and time coincidence are those acquired on the two aircraft flight legs between Dakar and Sao Paulo, however, the range of CO mixing ratios and the variety of conditions is increased if the data from all four legs are used. We have averaged each of the data sets over 5° x 5° latitude-longitude squares, and the results from the two instruments are shown in Table 7. Based on the data from the 15 grid squares in which both spacecraft and aircraft data were obtained, the spacecraft instrument yielded CO mixing ratios that were consistently about 45 percent lower than the mixing ratios measured by the aircraft system. As noted earlier, it appears that the spacecraft values were

about 30 percent lower than the values determined during the underflights by the Convair 990. In reporting the data from the 1981 MAPS flight (Reichle et al., 1986), the spacecraft data were compared to direct measurements obtained over Australia by Rasmussen et al. [1982], and the spacecraft were found to be about 20 percent low compared to the aircraft measurements. This change in the comparison from being about 20 percent low in 1981 to being 30 to 45 percent low in 1984 was a cause for great concern. We thoroughly reviewed and compared the MAPS data and procedures for each flight at each step of the data reduction process and found no discrepancies that would have caused this. It is now our conclusion that the errors in the satellite measurements were consistent between the two flights, and the apparent changes resulted from differences in the calibration standards among the various direct measurements systems. Further evidence of this is presented by Fraser et al. [1986]. They report that measurements taken by both Rasmussen and Seiler during the same month in 1982 at Cape Point South Africa show Rasmussen's standard yielding lower values. This is qualitatively consistent with our results.

Based on the data presented here and in our earlier paper, we now conclude that the MAPS measurements are consistently lower than near coincident direct measurements by from 20 to 45 percent, but the exact amount of the error can not be determined until the differences in the calibration standards for the various direct measurement systems are understood and eliminated. Since the MAPS data are acquired by a single instrument using consistent calibration and data reduction procedures, we believe that they are internally consistent and properly show the patterns and gradients in the global scale CO distribution even if the absolute values measured are found to be consistently low.

Results

Overview

About 85 hours of high-quality data were collected by the MAPS experiment over the 9 days of the flight. While some data were collected every day of the mission, the majority of the data were collected on October 6, 7, 8, 11, 12, and 13. These data have been averaged over 5° x 5° latitude-longitude squares and are shown in Figure 7a through 7f. The data for all 9 days of the flight have been further averaged and are shown in Figure 8.

Several features of the overall pattern of the data are noteworthy. In particular, certain regions showed very little change during the flight while others changed significantly.

The mixing ratio over the central Pacific Ocean is low and very uniform. The measured mixing ratios were usually 45 ppbv or less between 20°N and 20°S and between 150°E and 120°W. While there were occasional data higher than this, the average over the entire 9 days, in this region was between 35 and 45 ppbv as is shown in Figure 8. A second region of low mixing ratios was found over northern Africa from about 15°N to 30°N and from 15°W to 60°E. The presence of low values over northwest Africa were confirmed by the previously discussed Frankfurt-Dakar aircraft flight of October 6. As is the case with the central Pacific region, these low values persisted on each day of the shuttle flight.

Africa south of the equator showed very high mixing ratios every day on which the region was sampled and, in fact, these were the highest values measured during the entire flight. The CO mixing ratios from this area were as much as three times as high as those measured over the Pacific Ocean or northern Africa. The measurements also indicate very high CO mixing ratios over South America from the equator to 20°S. These values were not quite as

high as those measured over southern Africa. The third area to show consistently high readings is over northeast Asia and the adjacent Pacific Ocean (from 40°N to the northern edge of the flight track and from 45°E to 175°W). The measurements obtained over this area were high on each spacecraft pass.

In contrast to the areas mentioned in the foregoing paragraphs, two areas showed relatively high variability during the flight. During the first two full days of data acquisition (October 6 and 7) the CO mixing ratios over western Europe were quite high. By the third day, October 8, they had dropped and were among the lowest measured at these latitudes. The second area of variable mixing ratio is southeast Australia and the adjacent Pacific Ocean.

Discussion

Tropical South America and tropical Africa are known to be areas of extensive biomass burning in the form of groundfires (Batchelder, 1967). Recent observations by Crutzen et al. [1985] have not only investigated these fires, but also indicated that they are the cause of significant increases in tropospheric ozone. Cros et al. [1987] have concluded that high values of tropospheric ozone observed at Brazzaville, Congo bewteen October 8 and 10, 1984 were associated with a dry haze transported from the south African tropics, and the high ozone values may have been associated with biomass burning.

It is now clear that the high values of CO mixing ratio observed by the MAPS experiment over southern Africa and northern South America are associated with the presence of very extensive ground fires. The astronauts aboard the shuttle observed fires in these regions, and they were able to photograph many fires along the southeast coast of Africa. Dr. Kathryn Sullivan (personal communication, 1984) reported that she counted up to 80 fires on a single pass up the southeast coast of Africa. Because the spacecraft is traveling at a

speed of seven and one half kilometers per second, it is very likely that many fires were missed in the count. Examination of the handheld photography, e.g., photograph S17-46-015 which was acquired as part of the Space Shuttle Earth Observations Project (SSEOP) and which is available from the EROS Data Center, shows that the previously burned areas were very much larger than the size of the fires at the time that the data were acquired. Based on this, it is probable that the high CO mixing ratios observed between October 6 and October 13 had been present for some time prior to the flight. Thus it is clear that there are significant sources of CO in the Southern Hemisphere that result from biomass burning. The widespread high mixing ratios observed during this flight support the premise that the magnitude of such a source is comparable to the estimates from fossil fuel combustion in the Northern Hemisphere (Logan et al., 1981).

The changing situation over Europe was confirmed by the underflights of the Lufthansa airfreighter. It measured high CO mixing ratios upon its departure late in the day of October 6 and very much reduced mixing ratios on its return on October 8. Other trace gas measurements taken aboard the aircraft (ozone, nitric oxide, and water vapor) indicate that the air over the eastern North Atlantic Ocean and Western Europe on October 8 had recently been transported from the stratosphere or upper troposphere resulting in a low CO mixing ratio.

During November 1981 the MAPS exeriment obtained about 12 hours of data between 37°N and 37°S latitude (Reichle et al., 1986). Those data also showed very low CO mixing ratios in the region of the equatorial Pacific Ocean. Both the 1981 and 1984 data showed high mixing ratios over the equatorial Atlantic Ocean with the region of highest mixing ratios being somewhat further north during 1981. During the 1981 flight, high mixing ratios were also observed

over eastern Asia near the northern limits of the flight track, i.e., near 35°N to 40°N. These high mixing ratios have been attributed to transport form regions to the south (Newell et al., 1988). In the case of the data presented here, it appears that CO measured at those latitudes is part of a larger region of high mixing ratios located further north.

Summary

The second flight of the MAPS experiment, which took place during early October 1984, has demostrated that precise global measurements of middle tropospheric CO are feasible. The data reduction scheme has been modified to incorporate a method for objectively moving cloud contaminated data thereby making practical the processing of large amounts of data. Because of an apparent disagreement among the calibrations of the various ground-based systems, it is not yet possible to properly assess the absolute accuracy of the system, but based on all comparisons made to date the MAPS measurements appear to be systematically too low by from 20 to 40 percent.

The data support the existence of a large source of CO from widespread biomass burning in the Tropics over South America and Africa, a finding somewhat similar to what was found in the 1981 data set. In addition the 1984 measurements show very high values over Asia and downward over the western Pacific Ocean. The data also illustrate the temporal variability (over a 9-day period) of CO concentration over Europe with relatively high concentrations measured during the first few days of the mission, and considerably lower values observed during the latter days of the flight. It is likely that the relatively low concentrations over Europe during this time resulted from the presence of upper tropospheric air or even air that had been recently transported from the stratosphere. Another curious feature is the persistence of relatively low CO concentrations over North America.

Hopefully, a more detailed analysis of the prevailing meteorological conditions will yield a meaningful explanation of such low concentrations over this industrialized region.

The data show that there are substantial gradients in the CO mixing ratio with both latitude and longitude. The general character of the data acquired in October 1984 is similar to that of the data acquired in November 1981, but there are differences in detail. Finally, it is clear that at certain times of the year there are globally significant anthropogenic sources of CO in the Southern Hemisphere.

References

Abel, P. G., P. J. Ellis, J. T. Houghton, G. Peckham, C. D. Rodgers, S. D. Smith, and E. J. Williamson, The selective chopper radiometer for Nimbus D, Proc. R. Soc., London, Ser A, 320, 35, 1970.

Batchelder, R. B., Spatial and temporal patterns of fire in the tropical world, paper presented at the 6th Annual Tall Timber Fires Ecology Conference, 1987.

Cros, B., R. Delmas, B. Clairac, J. Loemba-Ndembi and J. Fontan, Survey of Ozone Concentrations in an Equatorial Region During the Rainy Season, J. Geophys. Res., 92, 9772, 1987

Crutzen, P. J., A. C. Delany, J. Greenburg, P. Haagenson, L. Heidt, R. Lueb, W. Pollock, W. Seiler, A. Wartburg, and P. Zimmerman: Observations of air composition in Brazil between the equator and 20°S during the dry season. J. Atmos. Chem., 2, 233-256, 1985.

Delany, A. C., P. J. Crutzen, P. Haagenson, S. Walters, and A. F. Wartburg, Photochemically produced ozone in the emission from large-scale tropical vegetation fires. J. Geophys. Res., 90, 2425-2529, 1985.

Fraser, P. J., P. Hyson, R. A. Rasmussen, A. J. Crawford, and M. A. K. Khalil, Methane, carbon monoxide, and methylchloroform in the southern hemisphere, J. Atmos. Chem., 4, 3, 1986.

Khalil, M. A. K., and R. A. Rasmussen, Carbon monoxide in the earth's atmosphere: Increasing trend, Science, 224, 54, 1984.

Khalil, M. A. K., and R. A. Rasmussen, Carbon monoxide in the earth's atmosphere: Indications of a global increase, Nature, 332, 242, 1988.

Logan, J. A., J. Prather, S. C. Wofsy, and M. B. McElroy, Tropospheric chemistry: A global perspective, J. Geophys. Res., 86, 7210, 1982.

Newell, R. E., S. T. Shipley, V. S. Connors, and H. G. Reichle, Jr.: Regional studies of potential carbon monoxide sources based on space shuttle and aircraft measurements, J. Atmos. Chem., 6, 61, 1988.

Rasmussen, R. A., M. A. K. Khalil, A. J. Crawford, and P. J. Fraser, Natural and anthropogenic trace gases in the southern hemisphere, Geophys. Res. Lett., 9, 704, 1982.

Reichle, Jr., H. G., V. S. Connors, J. A. Holland, W. D. Hypes, H. A. Wallio, J. C. Casas, B. B. Gormsen, M. S. Saylor, and W. D. Hesketh, Middle and upper tropospheric carbon monoxide mixing ratios as measured by a satellite borne remote sensor during November 1981, J. Geophys. Res., 91, 10865, 1986.

Rinsland, C. P., and J. S. Levine, Free tropospheric carbon monoxide concentrations in 1950 and 1951 deduced from infrared total column amount measurements, Nature, 318, 250, 1985.

Seiler, W., The cycle of atmospheric CO, Tellus, 26, 116, 1974.

Seiler, W., Measurement of the global distribution of tropospheric trace gases and their time dependent variations, final report No. KBF64, pp. 215, in press, BPT-publications, Munich, FRG, July 1988.

Seiler, W., J. Giehl, E. Brunke, and E. Holliday, The seasonality of CO abundance in the southern hemisphere, Tellus, 36B, 219, 1984.

Wallio, H. A., J. C. Casas, B. B. Gormsen, H. G. Reichle, Jr., and M. S. Saylor, Carbon monoxide mixing ratio inference from gas filter radiometer data, Appl. Opt., 21, 749, 1983.

Ward, T. V., and H. H. Zwick, Gas cell correlation spectrometer: GASPEC, Appl. Opt., 14, 2896, 1975.

Weiss, R. F., The temporal and spatial distribution of tropospheric nitrous oxide, J. Geophys. Res., 86, 7185, 1981.

J. C. Casas, SpaceTec Ventures, Incorporated, 17 Research Drive, Hampton, VA 23665.

V. S. Connors, H. G. Reichle, Jr., and H. A. Wallio, Atmospheric Sciences Division, Mail Stop 401A, NASA Langley Research Center, Hampton, VA 23665.

B. B. Gormsen, ST Systems Corporation, 28 Research Drive, Hampton, VA 23665.

J. A. Holland, Flight Electronics Division, Mail Stop 474, NASA Langley Research Center, Hampton, VA 23665.

R. T. Sherrill, Systems Engineering Division, Mail Stop 433, NASA Langley Research Center, Hampton, VA 23665.

Figure Legends

Figure 1. Schematic diagram of a gas filter radiometer.

Figure 2. Photograph of the instrument showing the various subassemblies.

Figure 3. Normalized MAPS signal functions for 50 ppbv carbon monoxide (solid curve) and 301 ppbv nitrous oxide (dashed curve).

Figure 4. Atmospheric models used in the data reduction (symbols as in Table 3)

(a) Temperature-pressure profiles;

(b) Water vapor-pressure profiles.

Figure 5. Number of N_2O data points inferred at a particular mixing ratio (dotted curve). Solid curve represents Gaussian fit.

Figure 6. (a) Unfiltered and (b) filtered carbon monoxide mixing ratios measured by the MAPS experiment on October 6, 1984 (c) from 20:05:00 to 21:40:00 UT.

Figure 7. Carbon monoxide mixing ratios averaged over 5° x 5° latitude-longitude grid squares.

(a) Data for October 6, 1984 (Day 280)

(b) Data for October 7, 1984 (Day 281)

(c) Data for October 8, 1984 (Day 282)

(d) Data for October 11, 1984 (Day 285)

(e) Data for October 12, 1984 (Day 286)

(f) Data for October 13, 1984 (Day 287)

Figure 8. Carbon monoxide mixing ratios averaged over 5° x 5° latitude-longitude grid squares for the period October 5 through October 13, 1984.

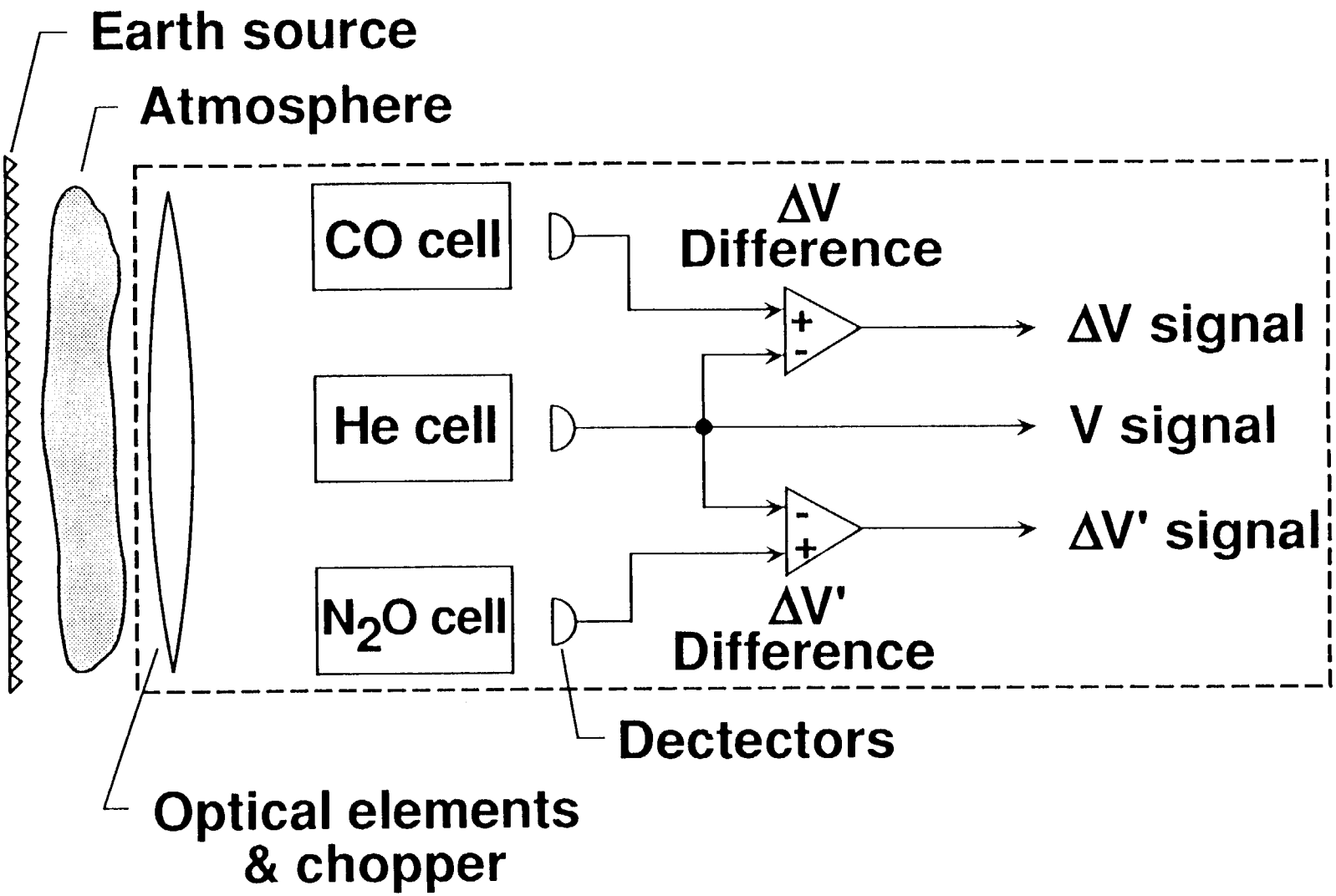
Earth source
Atmosphere
CO cell
He cell
N_2O cell
ΔV
Difference
+
-
ΔV signal
V signal
-
+
ΔV' signal
ΔV'
Difference
Dectectors
Optical elements
& chopper

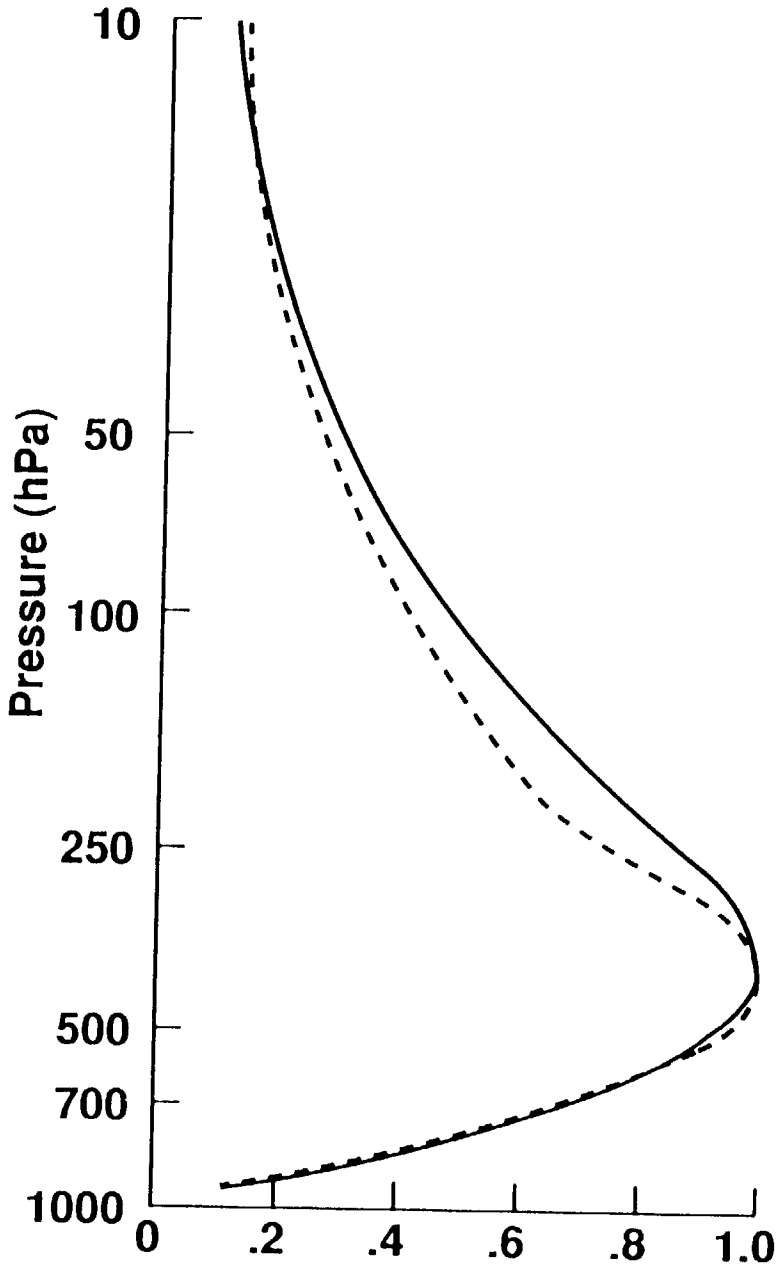
10
50
100
250
500
700
1000
Pressure (hPa)
0
.2
.4
.6
.8
1.0

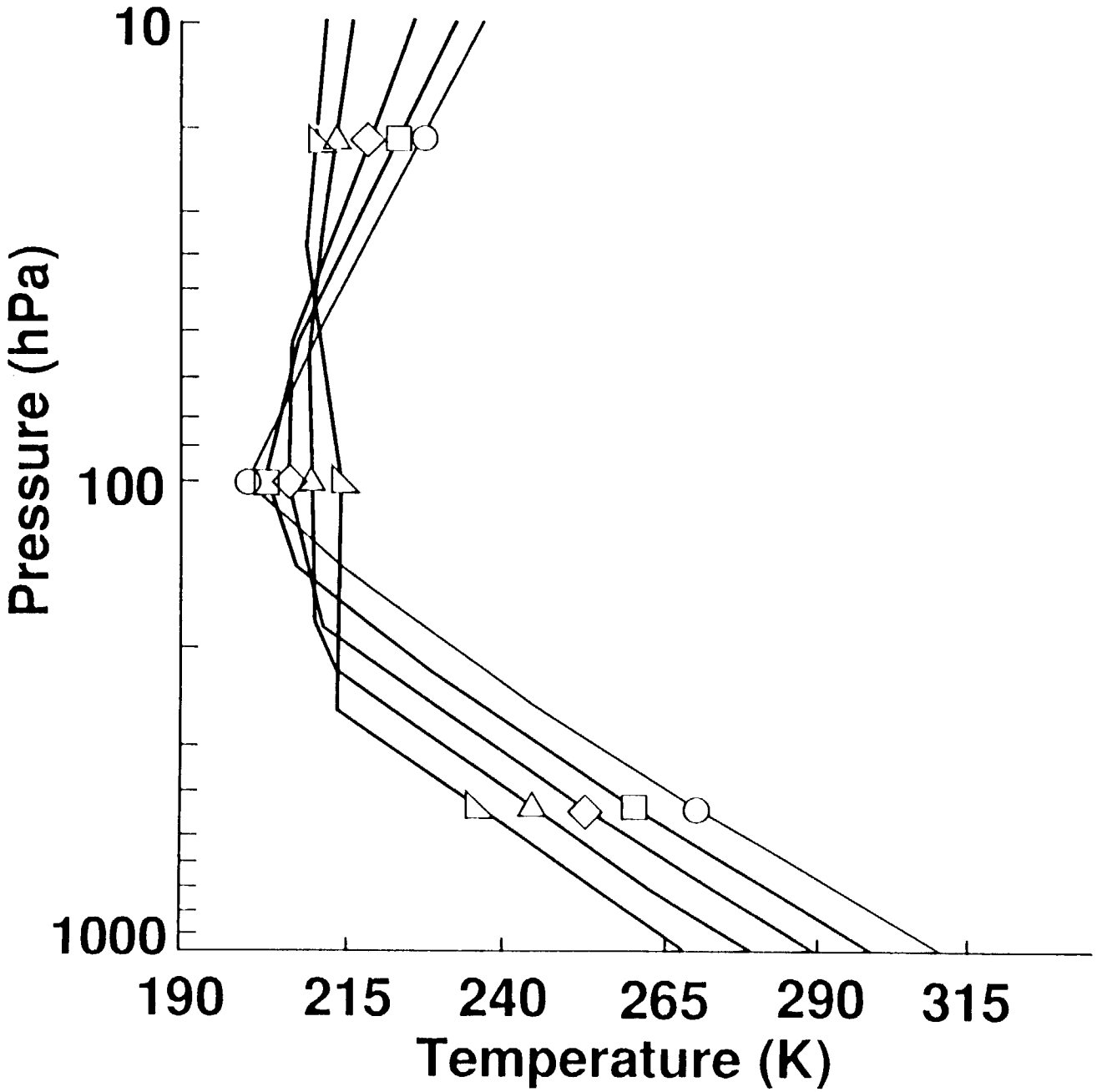
10
100
1000
Pressure (hPa)
190
215
240
265
290
315
Temperature (K)

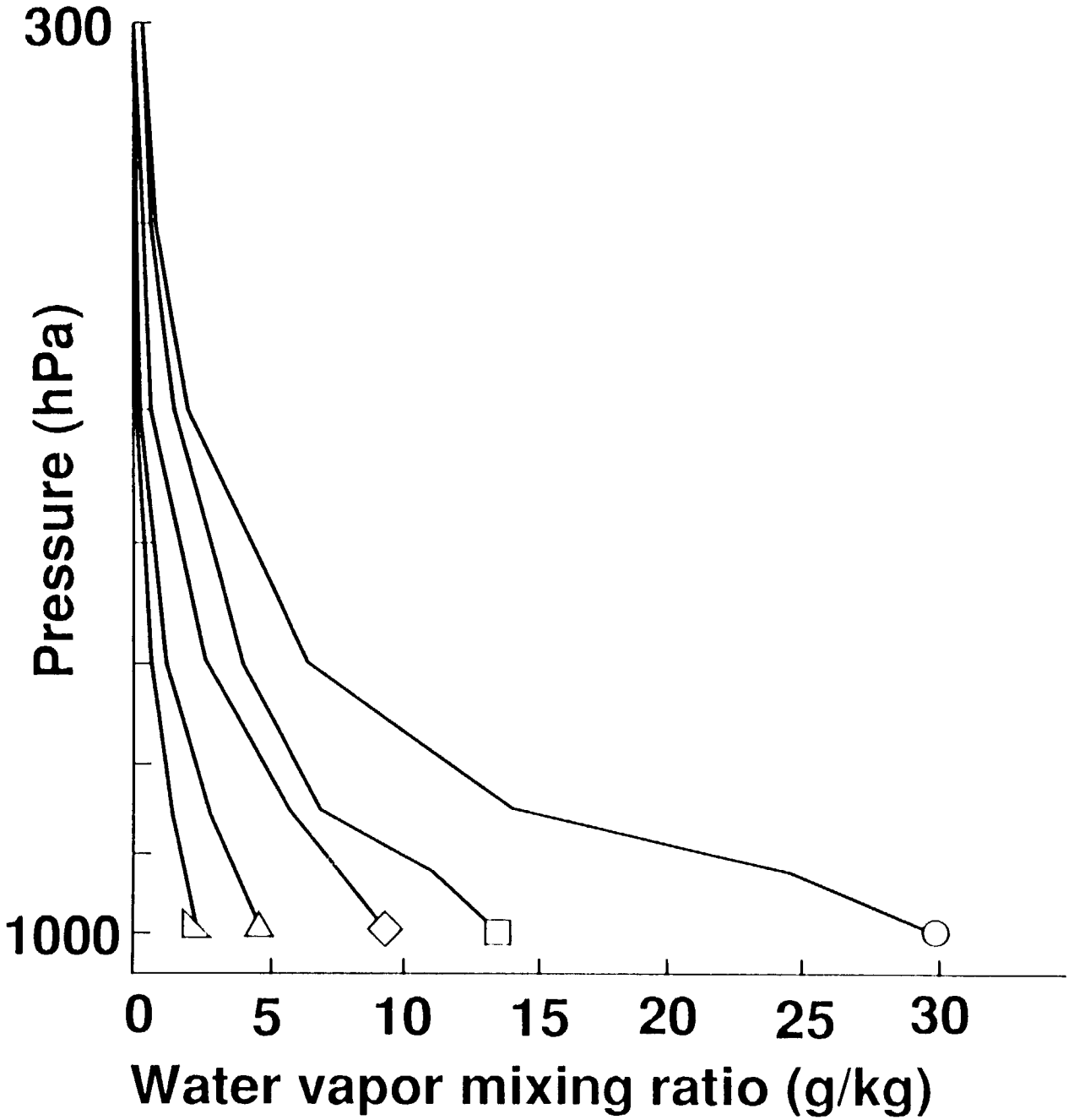
300
1000
Pressure (hPa)
0
5
10
15
20
25
30
Water vapor mixing ratio (g/kg)

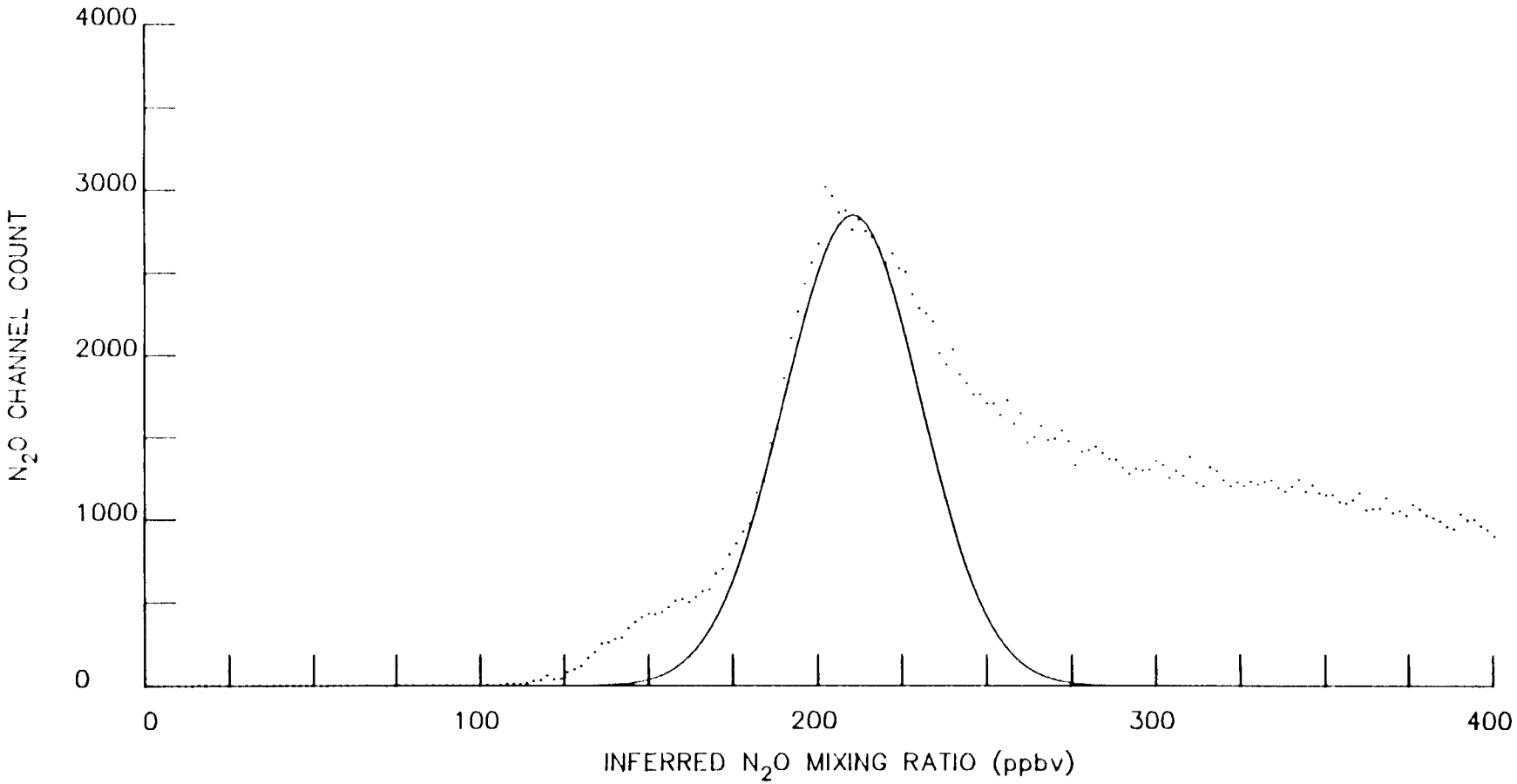
4000
3000
2000
1000
0
N_2O CHANNEL COUNT
0
100
200
300
400
INFERRED N_2O MIXING RATIO (ppbv)

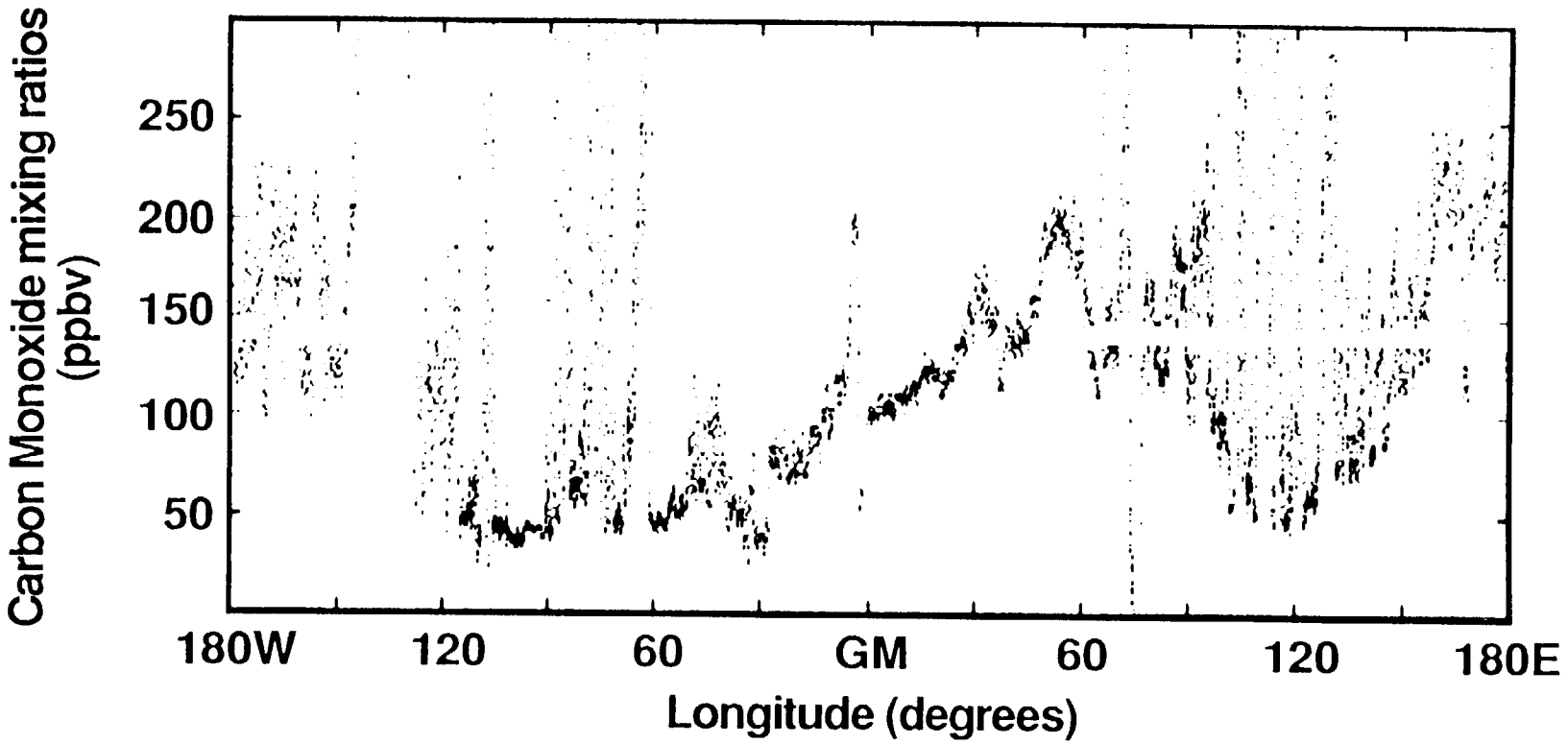
Carbon Monoxide mixing ratios (ppbv)
250
200
150
100
50
180W
120
60
GM
60
120
180E
Longitude (degrees)

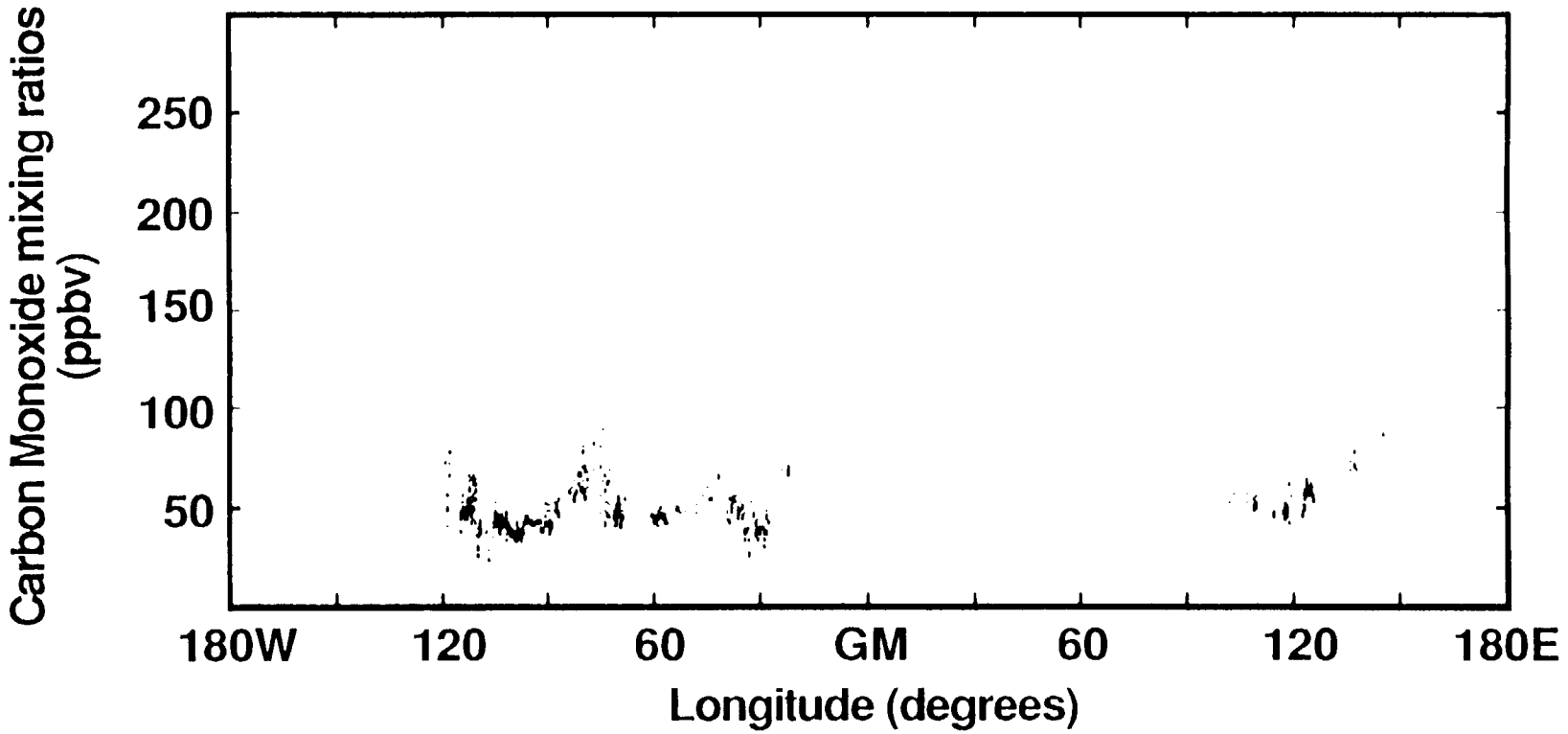
Carbon Monoxide mixing ratios (ppbv)
250
200
150
100
50
180W
120
60
GM
60
120
180E
Longitude (degrees)

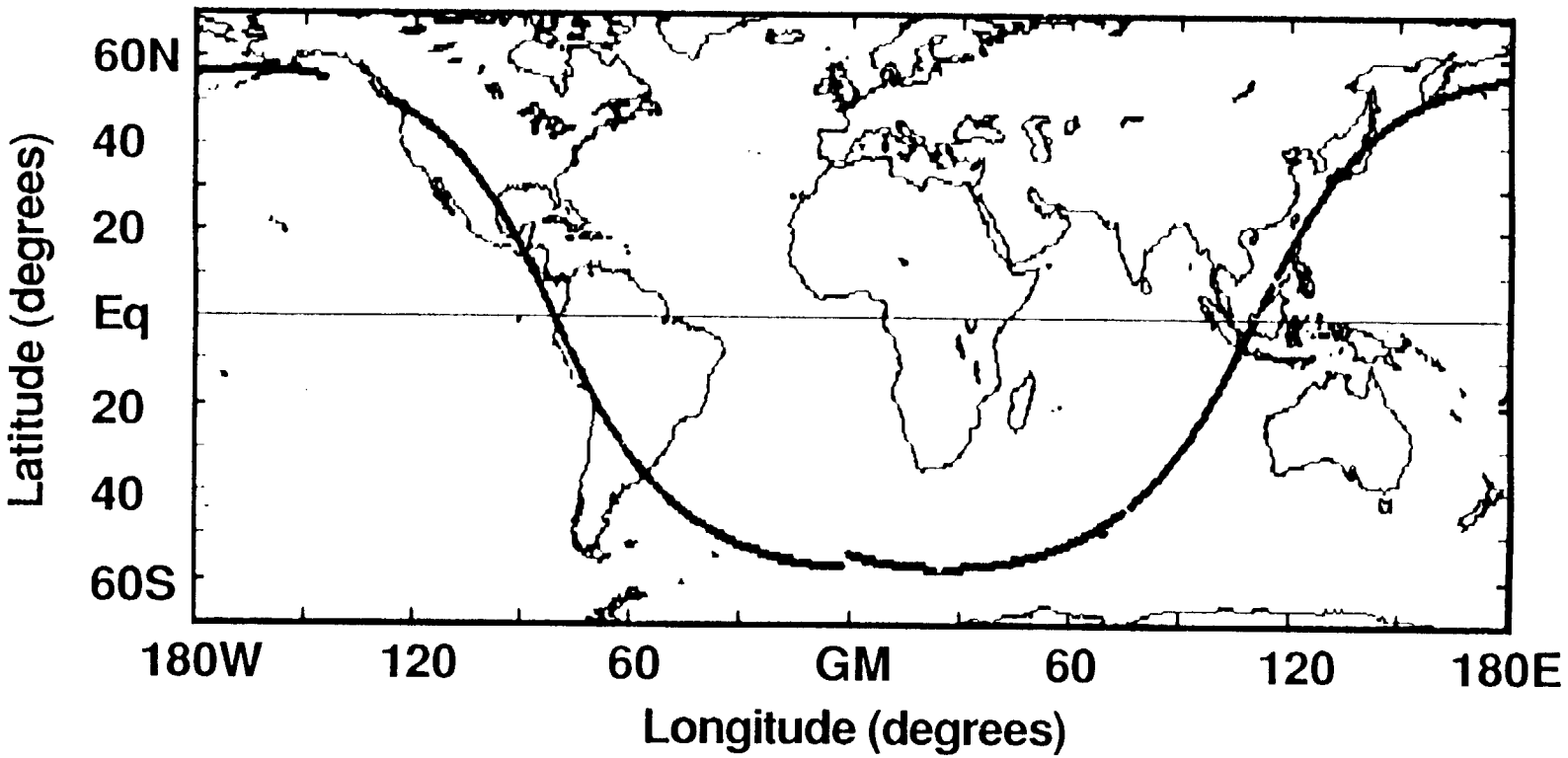
60N
40
20
Eq
20
40
60S
Latitude (degrees)
180W
120
60
GM
60
120
180E
Longitude (degrees)

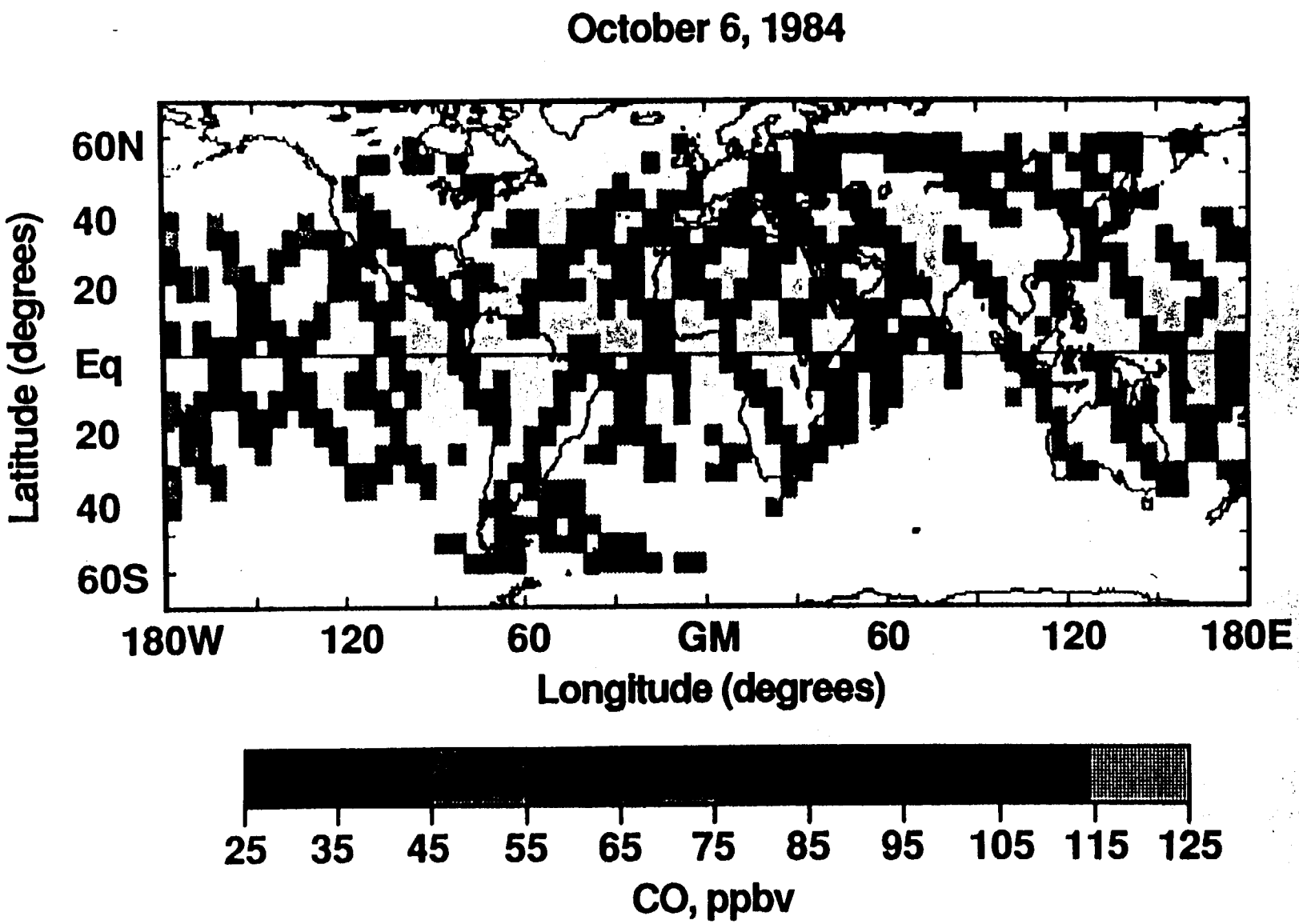
October 6, 1984
60N
40
20
Eq
20
40
60S
Latitude (degrees)
180W
120
60
GM
60
120
180E
Longitude (degrees)
25
35
45
55
65
75
85
95
105
115
125
CO, ppbv

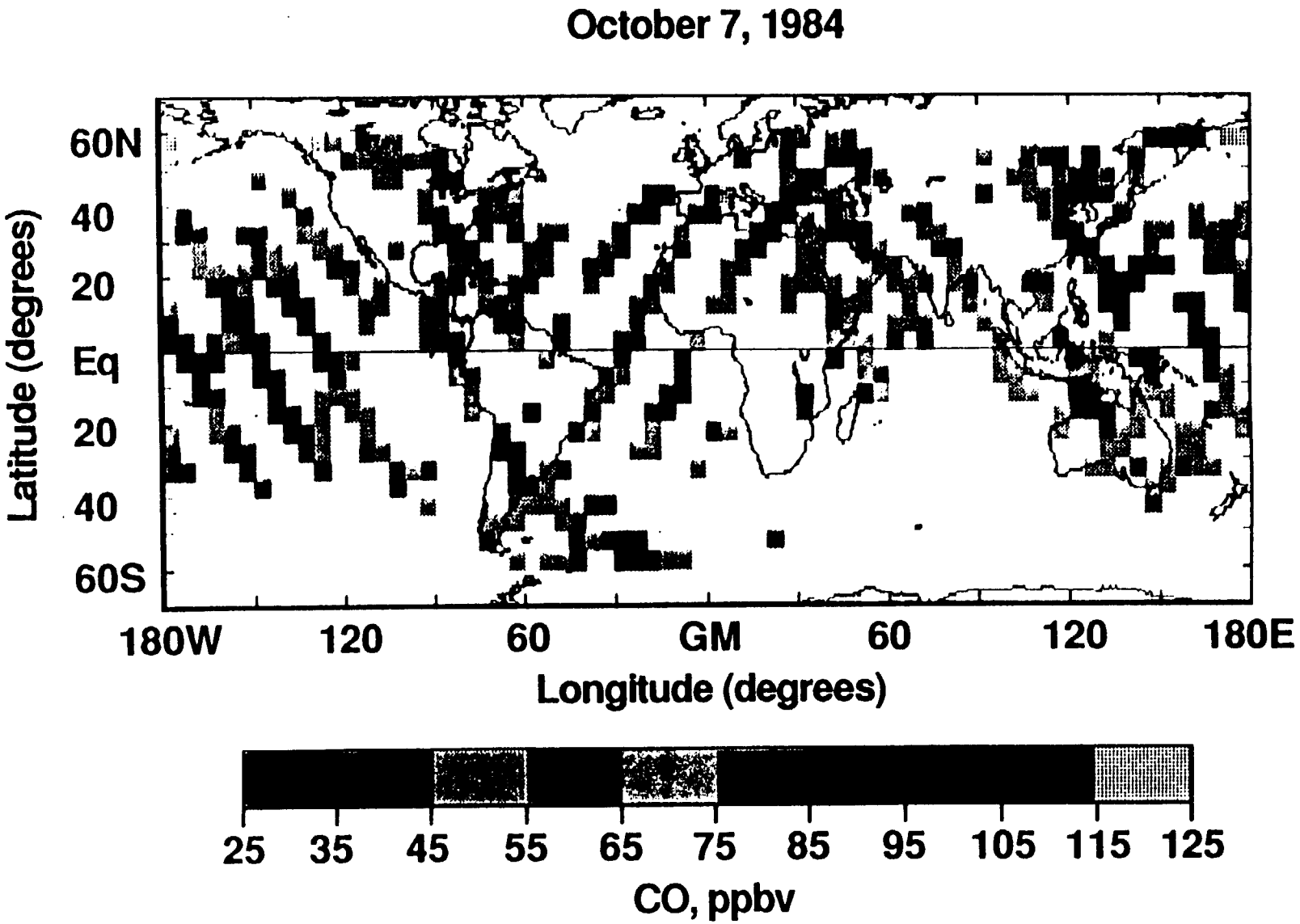
October 7, 1984
60N
40
20
Eq
20
40
60S
Latitude (degrees)
180W
120
60
GM
60
120
180E
Longitude (degrees)
25
35
45
55
65
75
85
95
105
115
125
CO, ppbv

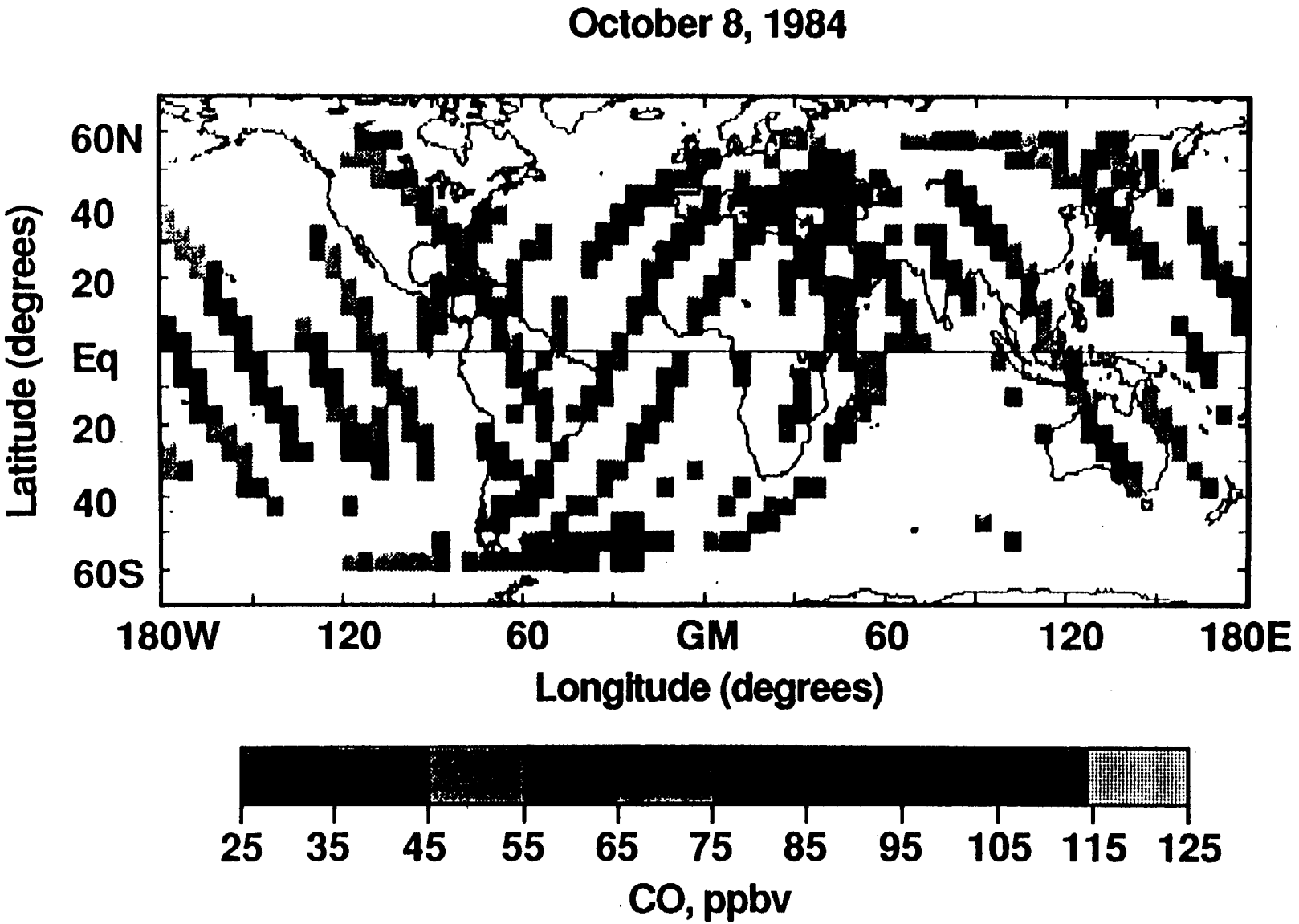
October 8, 1984
60N
40
20
Eq
20
40
60S
Latitude (degrees)
180W
120
60
GM
60
120
180E
Longitude (degrees)
25
35
45
55
65
75
85
95
105
115
125
CO, ppbv

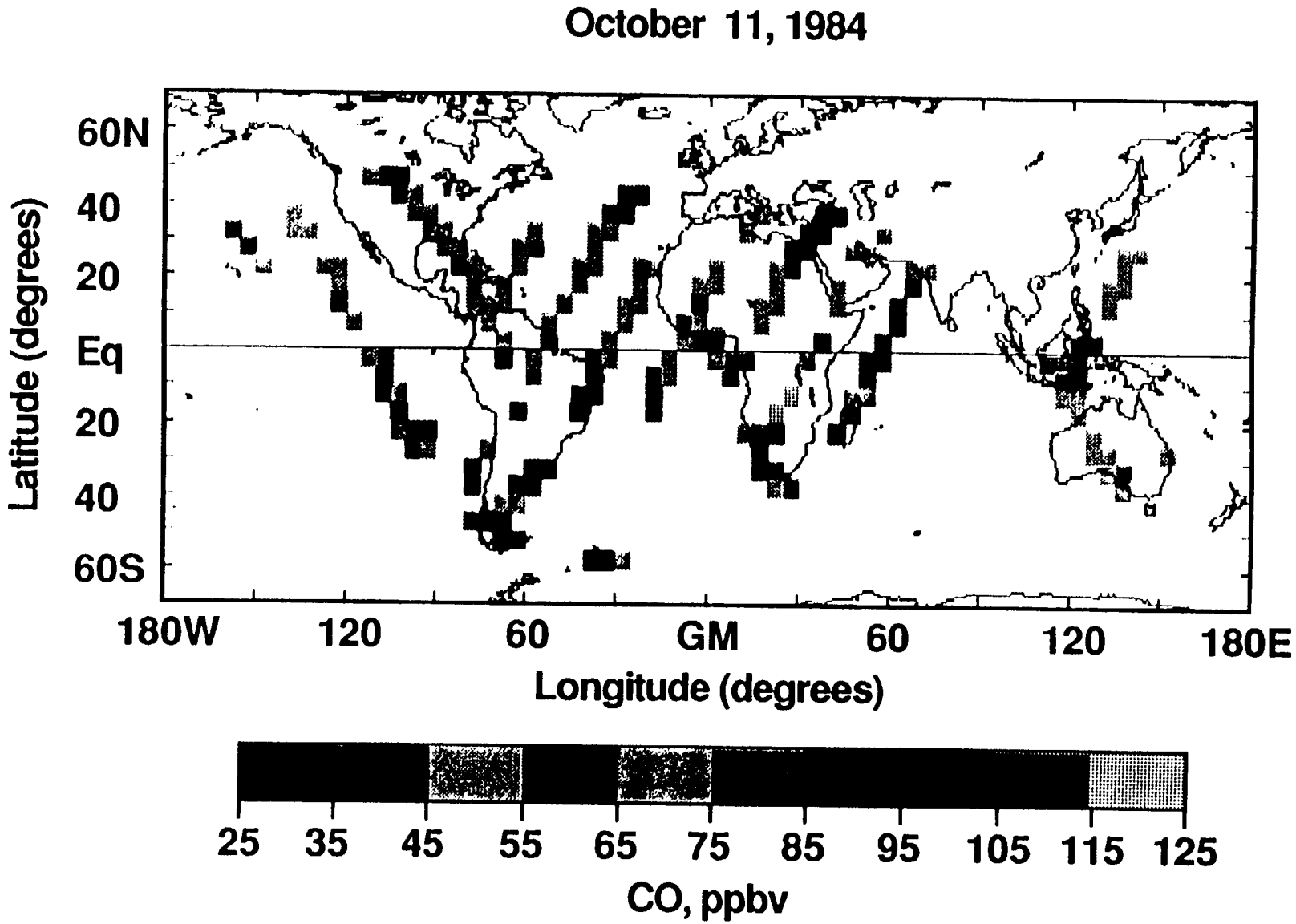
October 11, 1984
60N
40
20
Eq
20
40
60S
Latitude (degrees)
180W
120
60
GM
60
120
180E
Longitude (degrees)
25
35
45
55
65
75
85
95
105
115
125
CO, ppbv

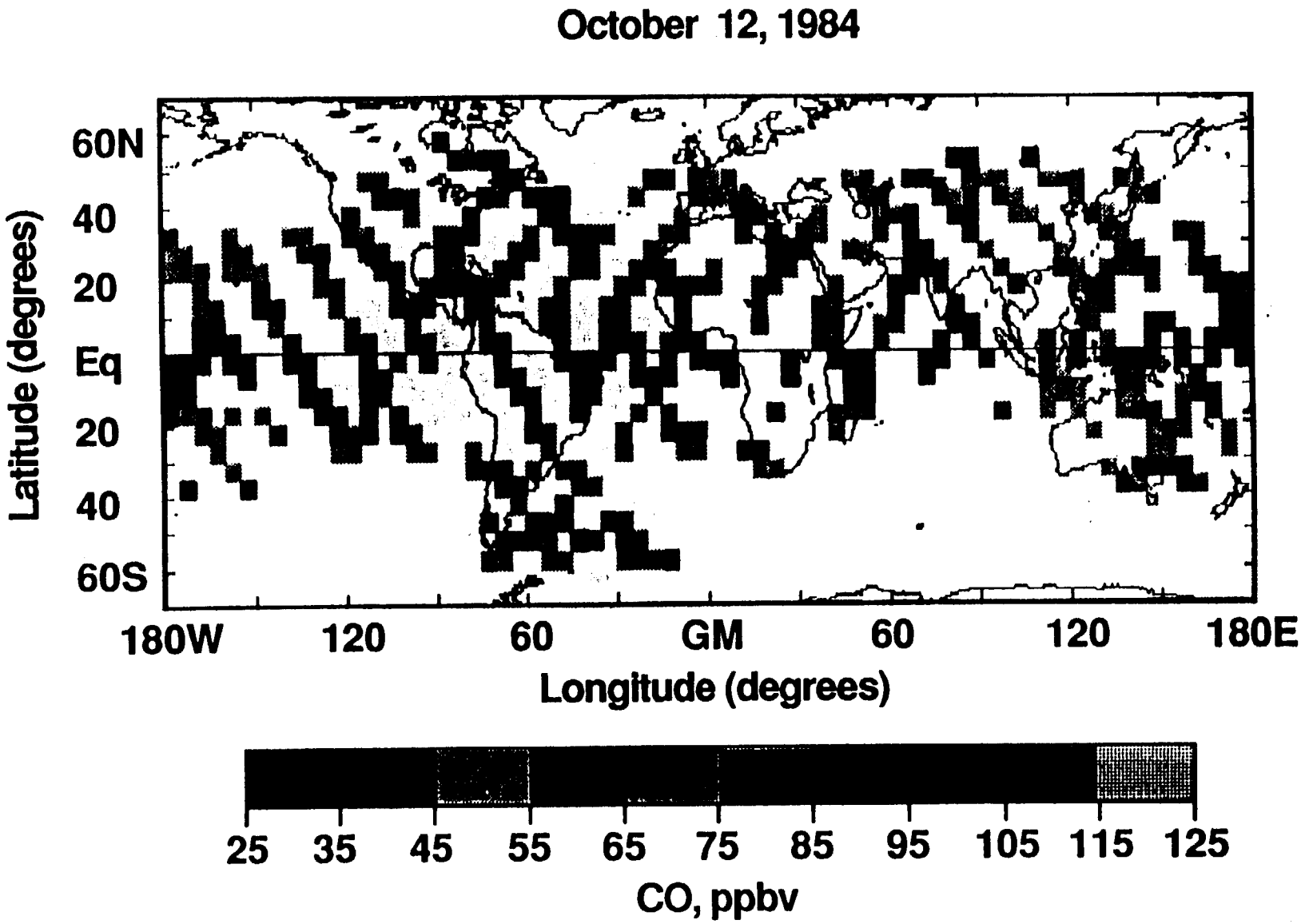
October 12, 1984
60N
40
20
Eq
20
40
60S
Latitude (degrees)
180W
120
60
GM
60
120
180E
Longitude (degrees)
25
35
45
55
65
75
85
95
105
115
125
CO, ppbv

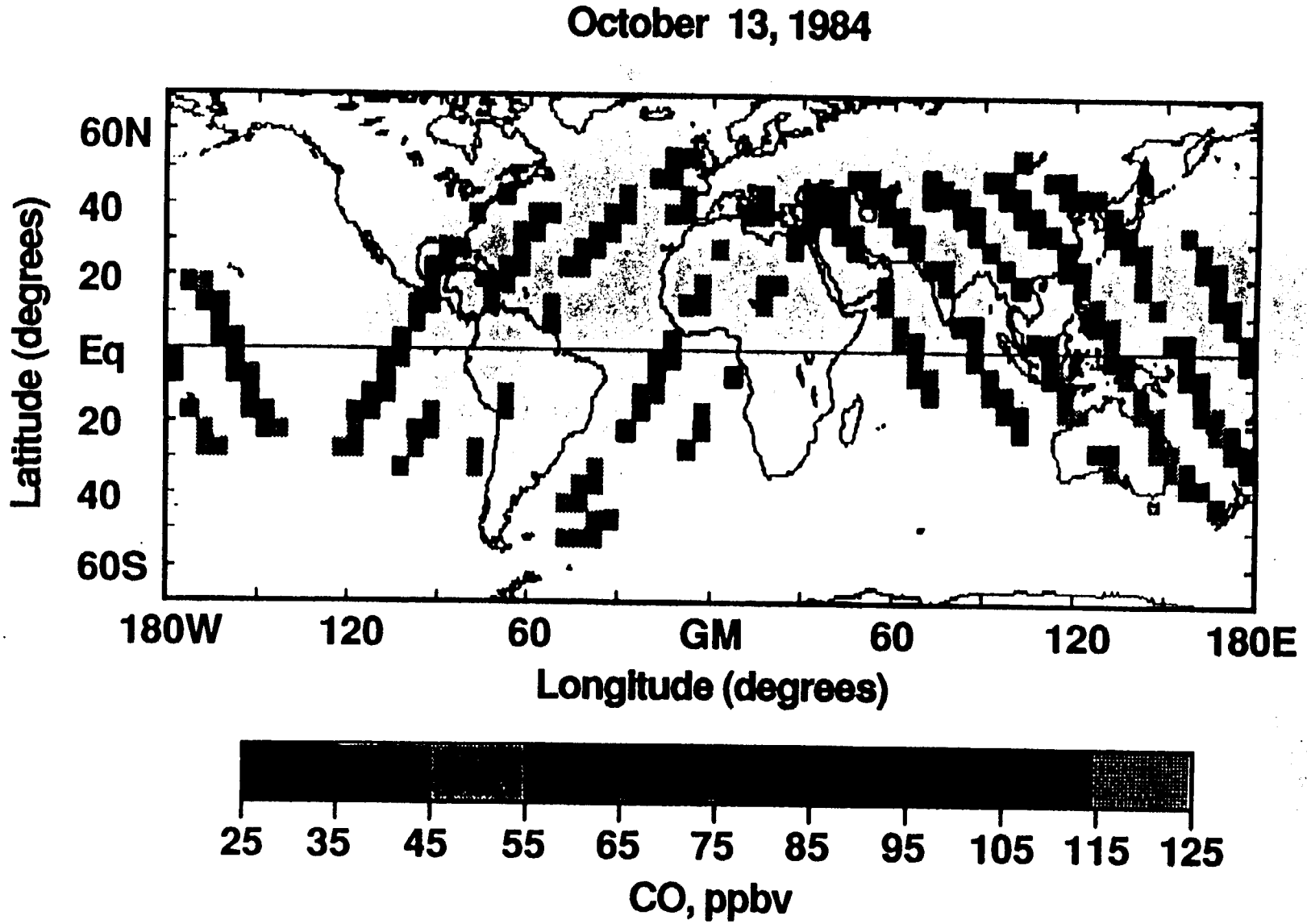
October 13, 1984
60N
40
20
Eq
20
40
60S
Latitude (degrees)
180W
120
60
GM
60
120
180E
Longitude (degrees)
25
35
45
55
65
75
85
95
105
115
125
CO, ppbv

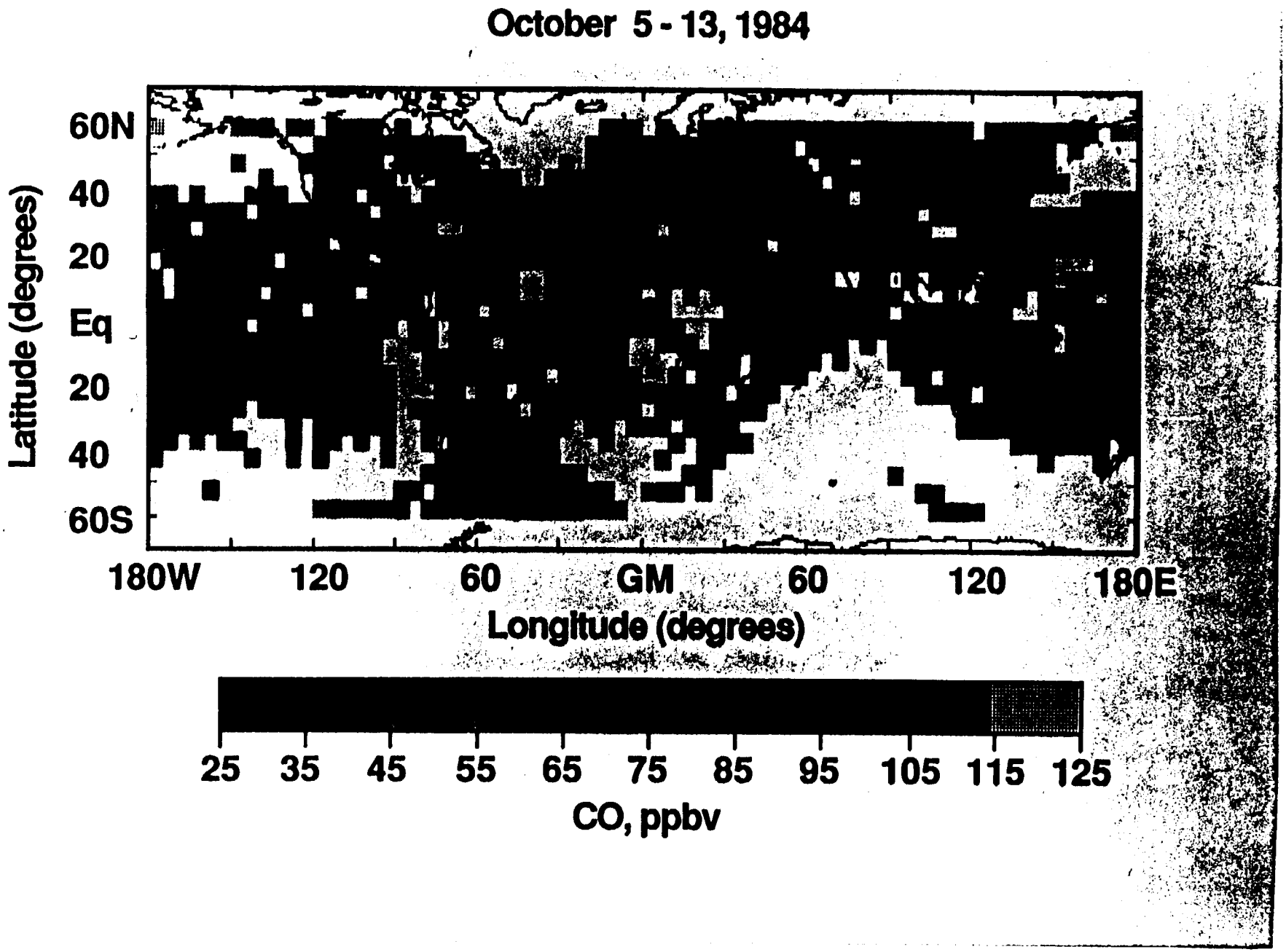
October 5 - 13, 1984
60N
40
20
Eq
20
40
60S
Latitude (degrees)
180W
120
60
GM
60
120
180E
Longitude (degrees)
25
35
45
55
65
75
85
95
105
115
125
CO, ppbv

TABLE 1. OSTA-3/MAPS Instrument Characteristics

Parameter	Value
Detected gas	Carbon monoxide
Spectral band	2080 to 2220 cm^{-1}
Detector type	PbSe, cooled to 195 K
FOV	4.33°
Entrance aperture	2.94 x 2.94 cm
Bandwidth	0.14 Hz
Gas cell pressure (Units: hPa)	CO / N_2O / He
Cell 1 ΔV'	0 / 149 / 3
Cell 2 ΔV	350 / 0 / 3
Cell 3 Vacuum	0 / 0 / 100
Calibrate	182 / 740 / 3
NEL V	1.7 x 10^{-7} W cm^{-2} sr^{-1}
ΔV, ΔV'	5.7 x 10^{-9} W cm^{-2} sr^{-1}
Size	0.90 x 0.76 x 0.56 meters
Mass	84 kg
Power, average in vacuum	73 W
Temperature range (baseplate)	273-288 K
Data rate	42 bits s^{-1}
Data storage	107 hours maximum
Camera	35 mm, aerial, 1 photo every 21 s when surface of Earth is illuminated
Film	Aerochrome 2443 false-color infrared

NEL is noise equivalent radiance.

TABLE 2. Test Conditions for Instrument Calibration

Instrument Temperatures, K	Secondary Standard Target Temperature Temperatures,* K	Secondary Standard Reference Cell Gas Mixtures Percent CO by Volume	Secondary Standard Reference Cell Gas Mixture Percent N_2O by Volume
272.6	273.7	2.5	5.0
272.7	280.0†	3.8	10.0
282.5	293.4	10.9	20.0
289.3	305.4		
	312.5		
	320.3†		

*Each target temperature and gas mixture was run at each instrument temperature.
†Target temperature equivalent to MAPS in-flight calibration blackbody temperatures.

Table 3

Characteristics of the atmospheric temperature models.

Model	Symbol	Surface	Tropopause	
		Temp. (K)	Temp. (K)	Height (KM)
A	○	310.0	196.3	17.5
B		306.0	200.4	17.1
C		302.5	199.0	16.8
D	□	299.0	204.0	16.5
E		295.0	210.3	13.8
F	◇	290.0	215.0	12.3
G		285.0	217.2	10.4
H	△	282.5	215.0	10.3
I		280.0	214.0	10.2
J		275.0	214.0	9.4
K	▷	270.0	214.8	8.5

Table 4

Theoretical Error Estimate for the CO Channel of the MAPS Experiment

Error Source	Magnitude of Perturbation	Random Error, %	Bias Error, %
Instrument Noise and temperature uncertainties	observed or estimated from flight data	±12	
Data Inversion			+0.5
Lorentz/Voigt			+0.5
Layering			+8.
Mixing layer	2 x Free Troposphere		-15 at 110 ppbv for cold atmosphere
Stratosphere	55 pbbv stratosphere, rather than uniformly mixed		-3 at 110 ppbv for tropical atmosphere
O_3	±20% of nominal	±2	
H_2O	25% of nominal to 90% relative humidity	±8	
Atmospheric temperature	±2K	±8	
Solar zenith angle and emissivity		±4	
Regression		±4	
		18*	0-6†

CO mixing ratio is 55 ppbv unless otherwise noted.
*Root-sum-square of random error.
†Total bias errors.

Table 5

Locations and carbon monoxide values obtained by the Convair 990 and Learjet correlative measurements flights

					CO (ppbv)		
Day	Flight	Lat.	Long.	Day / Night	S/C GFR	A/C GFR	GRAB SAMPLES MEAN/STD. DEV.
Oct. 7	Lear 1	25 N	79 W	Night	52	45	--
Oct. 8	Lear 2	25 N	81 W	Night	53	45	--
Oct. 8	Lear 3	25 N	79 W	Day	54	56	--
Oct. 9	Lear 4	25 N	82 W	Night	42	36	--
Oct. 10	Lear 5	27 N	83 W	Day	43	32	--
Oct. 12	Lear 7	28 N	84 W	Night	53	40	--
Oct. 13	Lear 8	29 N	84 W	Night	52	41	--
Oct. 6	Convair 1	35 N	105 W	Day	44	--	74/7.5
Oct. 7	Convair 2	28 N	125 W	Day	64	--	79/11.

Table 6

Times of data acquisition for the Frankfurt to Sao Paulo and return aircraft underflight.

Aircraft Flight Leg	Time of Aircraft Data, U.T.		Time of Spacecraft Data, U.T.	
Frankfurt - Dakar	Oct. 6	19:38-23:50	Oct. 6	11:45-16:45
Dakar - Sao Paulo	Oct. 7	01:49-07:28	Oct. 7	05:20-05:45
Sao Paulo - Dakar	Oct. 8	00:19-05:30	Oct. 8	05:03-05:18
Dakar - Frankfurt	Oct. 8	08:23-13:06	Oct. 8	06:50-07:05

Table 7

Carbon monoxide mixing ratios averaged over 5 degree latitude by 5 degree longitude grid squares as measured by the MAPS instrument and the Fraunhofer Research Institute-Lufthansa aircraft.

Lat/Long. of N.W. Corner of square	Date	MAPS CO	Aircraft CO (ppbv)	MAPS CO / A/C CO (ppbv)
35/-10	Oct. 6	38	84	0.45
10/-25	Oct. 7	53	90	0.59
5/-30	"	59	98	0.60
5/-25	"	56	101	0.55
0/-30	"	56	99	0.57
-5/-35	"	56	99	0.57
-5/-35	Oct. 8	52	92	0.57
0/-35	"	53	88	0.60
0/-30	"	53	92	0.58
5/-30	"	53	96	0.55
10/-25	"	51	95	0.54
15/-25	"	48	99	0.48
15/-20	"	50	101	0.50
25/-20	"	47	77	0.61
30/-15	"	40	76	0.53
			Mean	0.55
			Std. Dev.	0.05